UNSYS digital

Journal of Unmanned System Technology

Novel Phase Error Compensation Algorithm for Direct Digital Synthesizer Chirp Generator in Synthetic Aperture Radar

Heein Yang[†], Yuta Izumi[‡], Josaphat Tetuko Sri Sumantyo[†]

[†]Center for Environmental Remote Sensing (CEReS), Chiba University, Japan.

[†]Josaphat Microwave Remote Sensing Laboratory (JMRSL), Chiba University, Japan.

[‡]Sato Laboratory, Graduate School of Environmental Studies, Tohoku University, Japan.

Abstract— This paper proposes a novel phase error compensation algorithm for the direct digital synthesizer (DDS) chirp generator of high-resolution synthetic aperture radar (SAR). The proposed compensation algorithm adopts the curve fitting method to calculate the error of transmission SAR signal called chirp. In addition, this paper proposes the polynomial modeling method during chirp generation stage to improve spectrum characteristics. The mathematical equations proposed in this paper indicate that the phase shift of chirp in time domain can be eliminated clearly. Simulation results show that the proposed compensation algorithm enhances the peak-to-side lobe ratio (PSLR) and the integrated side ratio (ISLR) up to -0.2068 dB and -0.1091 dB respectively. In addition, spur components have been reduced when compared to the spectrum output of conventional DDS output.

Keywords— Synthetic Aperture Radar, Direct Digital Synthesizer, Linear Frequency Modulation, Chirp Signal, Phase Error Compensation

DOI: 10.21535/just.v6i1.1006

I. INTRODUCTION

THE synthetic aperture radar (SAR) provides the high resolution image of target in remote area regardless of the weather and day-light conditions [1]. Therefore, research issues to enhance the image quality and resolution of SAR are being remarkably handled. The general design requirements of radar system are the long detection range and the high resolution image of target. To achieve these requirements, radar system should support high transmission power and short pulse length. However, designing the radar system that satisfies those requirements is complicated due to the physical limitations. The resolution of radar system is inverse proportional to the signal bandwidth, therefore SAR adopts the linearly frequency modulated (LFM) signal called chirp instead of transmitting the high powered short pulse. The chirp has relatively long pulse length and low peak power but it generates the high resolution image of interested area by expanding the signal bandwidth. Because the instantaneous frequency of chirp increases according to the time variable, the chirp is able to provide wide bandwidth compared to single-tone sinusoid [2]. On the post processing stage, the SAR image processor operates pulse compression between chirp and the back-scattered signal from target. To obtain clear images, SAR should generate chirp as ideal as possible to obtain clear images. Recently, the design requirement on bandwidth has been increased up to 300–500 MHz to provide the sub-meter resolution (less than 1 m) [3].

Until now, several types of chirp generators have been introduced such as frequency multiplier, the memory-map generator, and the direct digital synthesizer (DDS) [4]. Among those signal generators, the memory-map based chirp generator shows ideal-like signal output. However, when it generates wideband chirp, it requires large memory capacity [5]. In the case of space-borne SAR, because of high energy particle of cosmic ray, the memory units are vulnerable. Therefore, signal generator that stores the whole predefined waveform data in PROM and reconstructs the signal might suffer from bit error problem easily. To reduce the memory dependency in space environment, the DDS chirp generator implemented on the field programmable gate array (FPGA) has been studying to be used on satellite on-board SAR [6].

Compared to the conventional phase-locked loop (PLL) based frequency synthesizers, the DDS has several advantages; the high-performance of frequency resolution, high speed switching, and *etc* [2]. When DDS generates the desired signal, it truncates some of expression bits [7]. Truncation process can reduce power consumption, however DDS output shows phase errors and spurious. Therefore, the time domain output shows phase error on the signal center and the frequency domain output shows low spectrum purity which leads to the waste of frequency resource. Those problems above are detailed in following sections. This paper proposes a novel phase error compensation algorithm for the FPGA based wideband chirp generator to enhance the performance of SAR.

Corresponding author: Heein Yang (e-mail: kfcddong@gmail.com)

This paper was submitted on April 19, 2018; revised on May 21, 2018; and accepted on May 22, 2018.

II. DDS Chirp Signal Generator

A. Mechanism of DDS Chirp Generator

DDS consists of digital counter and adder which work as accumulator and look-up table (LUT) [5]. The DDS chirp generator has two accumulators in a row and it generates the phase of desired waveform. LUT stores the amplitude information of sinusoid and reconstructs output signal by matching the amplitude according to the phase address. Figure 1 shows the functional block diagram of DDS chirp generator. It consists of the amplitude and phase accumulators, LUT, digital-to-analog converter (DAC), and clock oscillator. Input signal, the N-bit frequency control word (FCW), is accumulated by each clock then DDS generates the phase of desired signal. The value of FCW indicates a step size of phase increment within the accumulator capacity. LUT that stores amplitude value of sinusoid reconstructs the desired signal according to the phase address from accumulator. A mathematical expression of the baseband ideal chirp $s_{(t)}$ is

$$s_{(t)}=\text{rect}\left(\frac{t}{T}\right)\exp\left(j\pi \mathrm{K}t^2\right) \tag{1}$$

where t, T, and K indicate the time variable, pulse width, and chirp rate, respectively. $\text{rect}\left(\frac{t}{T}\right)$ yields 1 where $\left|\frac{t}{T}\right| \le \frac{1}{2}$ [8]. Equation (1) indicates that the instantaneous frequency of chirp varies with K linearly within time t. Therefore, the bandwidth of chirp equals to Kt. To investigate the phase and frequency components of chirp signal, (2) and (3) are shown as

$$\phi_{(t)} = \pi \mathrm{K}t^2 \tag{2}$$

$$f_{(t)} = \frac{1}{2\pi}\frac{d\phi(t)}{dt} = \mathrm{K}t \tag{3}$$

B. Problems of conventional chirp generator

Since DDS operates in digital circuit, we express some important discrete chirp parameters below [1]. This paper assumes that FCW is N-bit long. When expressing the clock frequency as f_{clk}, the frequency resolution Δf and the maximum output frequency f_{max} are defined as

$$\Delta f = \frac{f_{\text{clk}}}{2^N} \tag{4}$$

$$f_{\text{max}} = \Delta f \cdot \text{FCW} = \frac{f_{\text{clk}} \cdot \text{FCW}}{2^N} \tag{5}$$

The accumulator of conventional DDS chirp generator accumulates the input (FCW) in every clock so that it can be considered as the time-integration operator. In every clock time, the accumulator accumulates input value continuously and overflows it when the accumulated output reaches its capacity value. When accumulator unit calculates continuously, the output overflows when it reaches 2π [9]. However, since DDS is a digital system, the overflow output truncates in the rising edge of clock signal. According to the phase wheel fundamental [2], the starting phase of each cycle does not equal to offset. Because of offset mismatch within each cycle, the conventional DDS has phase error in its time domain signal center. Because the proposed DDS is implemented with N-bit, the overflow value is evenly spaced by 2^N within $[0,2\pi)$.

$$f_{\text{FA}(t)} = \left(\frac{\text{FCW}}{2^N}\cdot t\right)\cdot 2^N \tag{6}$$

$$\phi_{\text{PA}(t)} = \frac{1}{2}\left(\frac{\text{FCW}}{2^N}\cdot t\right)^2 \cdot \frac{2^N}{2^p} \tag{7}$$

where $f_{\text{FA}(t)}$, $\phi_{\text{FA}(t)}$, and p are the output from frequency and phase accumulators, and p-truncated bit respectively.

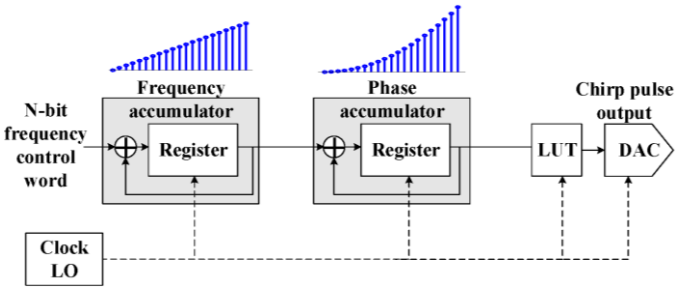

Figure 1 Functional block diagram of DDS chirp generator

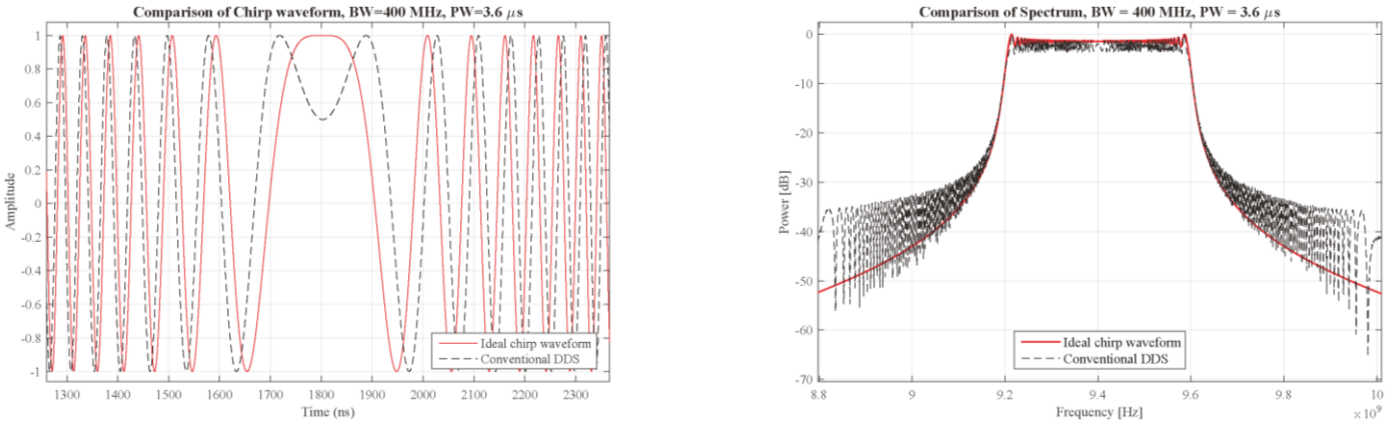

(a) **(b)**

Figure 2 Ideal chirp and conventional DDS output.
(a) Time domain chirp; (b) Spectrum output

Figure 2(a) and Figure 2(b) show the comparison of time and frequency domain output between ideal chirp and conventional DDS output. In Figure 2(a), the solid line and the dashed line represent the ideal chirp waveform and the conventional DDS chirp output in time domain, respectively. As expressed in **(1)**, the real part of chirp signal has cosine term, therefore the time domain waveform should have the cosine waveform characteristics. However, the signal center of DDS output shows slight phase shift. This phenomenon leads to spurious shown in Figure 2(b). Solid line in Figure 2(b), the idea chirp waveform in frequency domain, attenuates ideally. DDS spectrum output also attenuates but spur exists such as spectral regrowth, ripple noise, and etc. To solve these problems, this paper proposes a novel phase error compensation algorithm using polynomial modeling that enhance the spectrum characteristic of DDS chirp generator.

III. Proposed Method

The proposed algorithm has two main features. Firstly, it applies the curve fitting method. Secondly, it calculate the error compensation coefficient, then compensates error on each accumulator block.

A. *Error modeling using polynomial*

During signal generation stage, each accumulator in DDS occurs residual offset error because of the roll-over in every overflow cycle [10]. We denote the residual error components of the frequency and phase accumulators as f_x and ϕ_x respectively. Using **(6)** and **(7)**, the output model of each accumulator can be expanded as

$$f_{\mathrm{FA}(t)} = \left(\frac{\mathrm{FCW}}{2^N} \cdot t \right) \cdot 2^N + f_x \tag{8}$$

$$\phi_{\mathrm{PA}(t)} = \left(\frac{1}{2} \left(\frac{\mathrm{FCW}}{2^N} \cdot t \right)^2 + \left(\frac{f_x}{2^N} \cdot t \right) + \frac{\phi_x}{2^N} \right) \cdot \frac{2^N}{2^P} \tag{9}$$

This paper denotes the phase error of DDS $\phi_{\mathrm{error}(t)}$ as

$$\phi_{\mathrm{error}(t)} = \phi_{(t)} - \frac{\phi_{\mathrm{PA}(t)}}{\left(\frac{2^N}{2^P} \right)} \tag{10}$$

To model the error from phase accumulator, we apply the curve fitting process on the DDS phase error $\phi_{\mathrm{error}(t)}$ using 2nd order polynomial $\phi_{\mathrm{cf}(t)}$ shown as

$$\phi_{\mathrm{cf}(t)} = \alpha t^2 + \beta t + \gamma \tag{11}$$

where α, β, γ indicate the quadrature, linear, and random error coefficients of conventional DDS respectively. The coefficients above will be used to compensate the residual error from DDS components.

B. *Error compensation using coefficients*

The compensated phase output of DDS $\phi_{\mathrm{comp}(t)}$ using proposed algorithm can be expressed as

$$\phi_{\mathrm{comp}(t)} = \frac{\phi_{\mathrm{PA}(t)}}{\left(\frac{2^N}{2^P} \right)} + \phi_{\mathrm{cf}(t)}$$

$$\phi_{\mathrm{comp}(t)} = \frac{\phi_{\mathrm{PA}(t)}}{\left(\frac{2^N}{2^P} \right)} + \left(\phi_{(t)} - \frac{\phi_{\mathrm{PA}(t)}}{\left(\frac{2^N}{2^P} \right)} \right) \tag{12}$$

From **(8)** and **(10)**, we can assure that the phase output of the proposed method theoretically compensates the error. After extracting the error compensation coefficients, we design the block diagram of the proposed error compensation algorithm.

Figure 3 shows that the phase output of DDS is processed with curve fitting to generate 2nd order polynomial model. Next, the ideal phase of chirp generated DDS IP core subtracts its signal with the DDS phase output. Last, we estimate the error compensation coefficients, then calculates the quadrature, linear, and random errors respectively. By differentiating $\phi_{\mathrm{cf}(t)}$, we divide each compensation coefficient according to the signal generation process of DDS. 2α, β, and γ compensate FCW error, the residual error of frequency and phase accumulators respectively.

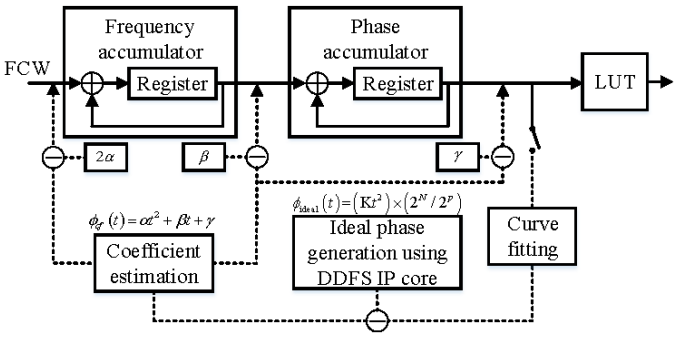

Figure 3 Block diagram of the proposed error compensation algorithm

IV. Performance Analysis

In this section, the impulse response function (IRF) and spectrum output comparison are analyzed to verify the feasibility of the proposed error compensation algorithm. In addition, we conduct the point target analysis simulation to verify the effect of phase error and proposed method on SAR image.

Table 1 Simulation environment of RF system

Parameters	Value
Center frequency	9.4 GHz (X-band)
Pulse width	3.6 μs
Bandwidth	±200 MHz from center frequency
HPA type	SSPA
Integrated phase noise	-60 dBc
Phase noise floor	-120 dBc/Hz

A. *Comparison of impulse response function and spectrum*

We investigate the peak-to-side lobe ratio (PSLR) and the integrated side lobe ratio (ISLR) from IRF. PSLR indicates the noise level between peak and side lobe. ISLR presents the proportion of energy between the main lobe and the side lobe from the first to 10th nulls on both side. To analyze the performance of proposed algorithm, this paper exploits the design parameters described in Table 1.

Figure 4(a) and Figure 4(b) show the IRF and spectrum output of the conventional DDS and the proposed method respectively. For the simulation, 400 MHz of chirp with 3.6 μs pulse width which is centered in 9.4 GHz has been generated. In both figures, the dashed line and the solid line indicate the graph of conventional DDS and the proposed method output respectively. The mathematical expressions of PSLR and ISLR are presented as

$$I_{PSLR} = I_{main}[dB] - I_x[dB] \quad \textbf{(13)}$$

$$I_{ISLR} = \frac{\int_{-1N}^{1N} \left|h_{(t)}\right|^2 dt}{\int_{-1N}^{-10N} \left|h_{(t)}\right|^2 dt + \int_{N}^{10N} \left|h_{(t)}\right|^2 dt} \quad \textbf{(14)}$$

where I_{main} and I_x are the peak value of main-lobe and side-lobe [1]. From Figure 4(a), the conventional DDS shows -13.3920 dB of PSLR and -10.0857 dB of ISLR. On the other hand, the DDS using proposed method shows higher PSLR and ISLR; -13.5688 dB and -10.1948 dB respectively. It means that IRF performance has been enhanced when using the proposed method. Table 2 shows the comparison of IRF output between the conventional and proposed DDS.

Table 2 Result of IRF analysis

Parameters	Conv.	Proposed	Enhancement
PSLR [dB]	-13.3920	-13.5688	-0.2068
ISLR [dB]	-10.0857	-10.1948	-0.1091

A comparison of spectrum output is shown in Figure 4(b). As shown in Figure 4(b), the conventional DDS shows spurs. However, the solid line in Figure 4(b) shows stable output compared to the conventional DDS output. We can assure that the proposed error compensation algorithm is able to reduce spur components in noise band.

B. *Point target analysis*

To verify the feasibility of proposed algorithm, this paper conducts point target analysis using the chirp from conventional DDS and the proposed DDS. In this simulation, we have one target in the center of interested area. The point target images are processed using the range Doppler algorithm (RDA) and the range cell migration (RCM) has been compensated. In addition, zero padding has been applied to obtain clear images.

Figure 5 shows the point target analysis results. Figure 5(a) and Figure 5(b) are the point target images when using the conventional DDS and the proposed DDS respectively. In both figures, the 2-dimensional point targets are shown along range and azimuth axis. The bright points in the center of Figure 5(a) and Figure 5(b) are considered as the main lobe of point target. We can find that side lobe exists from the main lobe and it can be considered as noise. In Figure 5(a), the fist null of side lobe near the main lobe cannot be distinguished clearly. However, Figure 5(b) shows that the border between main lobe and side lobe can be discriminated clearly compared to the conventional DDS output. From results above, we can assure that the proposed DDS can reduce the noise near point target and it can enhance the image quality. To compare the point target analysis result using amplitude value, Figure 5(c) and Figure 5(d) are shown. We capture the signal strength from point target along the standard azimuth line. Figure 5(c) and Figure 5(d) show the IRF of conventional DDS and proposed method respectively. Figure 5(d), the target amplitude of proposed DDS, shows less noise on side lobes when compared to Figure 5(c). It shows that the proposed error compensation algorithm is able to enhance the point target image quality.

Figure 5(e) and Figure 5(f) are shown to compare the image quality enhancement when there are multiple targets in the area of interest. We plot four-point-taget in the field and conduct the same procedure of point target analysis. The points captured in this simulation are the outer sidelobe of overlapped point targets. The amplitude level of Figure 5(e) and Figure 5(f) show 4214 and 3848 respectively. It indicates that the proposed algorithm is able to suppress the outer sidelobes where there are two or more targets in the area. Similarly, we plot the inner sidelobe level in Figure 5(g) and Figure 5(h). In case of conventional DDS, the inner sidelobe level shows -15.57 dB while the proposed DDS shows -16.61 dB. We could suppress the inner sidelobe up to -1.04 dB when using the proposed phase error compensation algorithm.

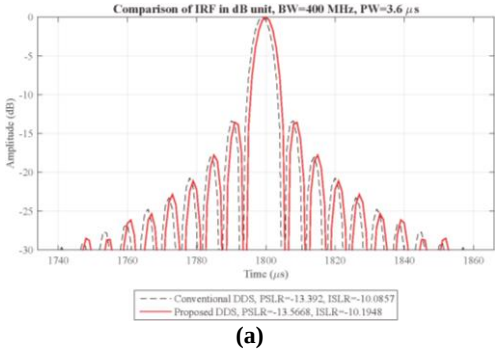

(a)

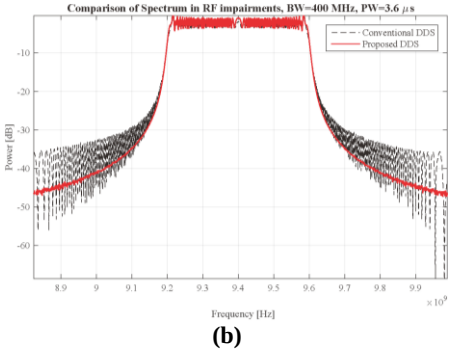

(b)

Figure 4 Conventional DDS and proposed DDS output: (a) IRF output; (b) Spectrum output

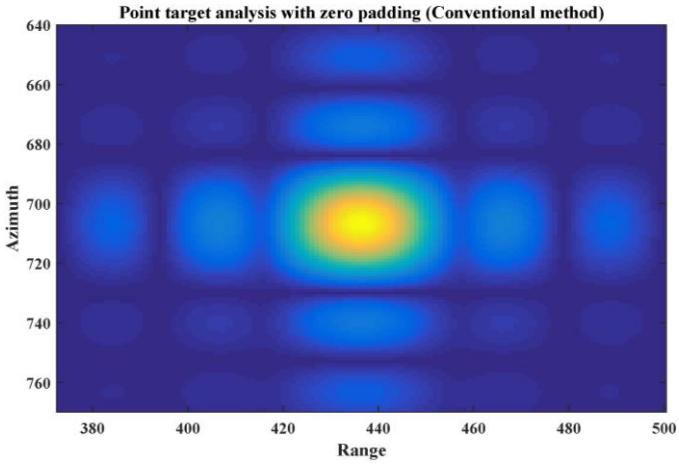
Point target analysis with zero padding (Conventional method)
Azimuth
Range

(a)

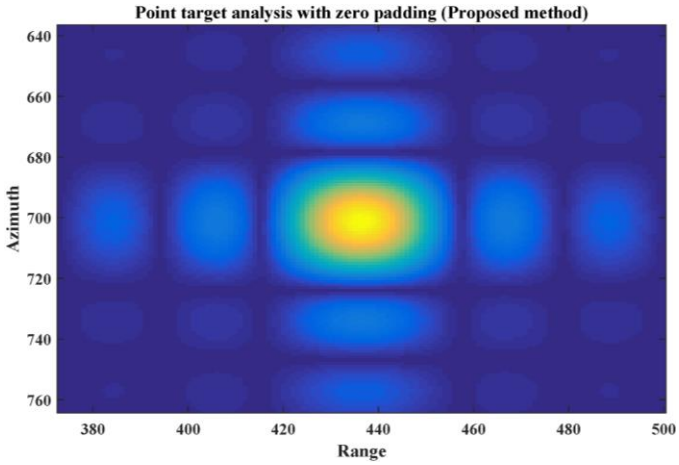
Point target analysis with zero padding (Proposed method)
Azimuth
Range

(b)

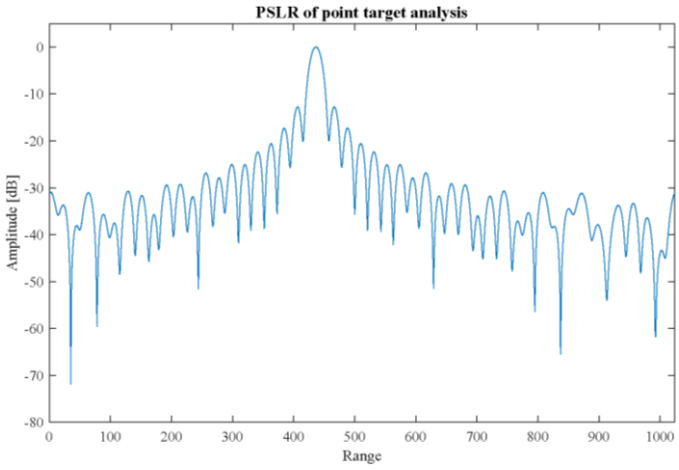
PSLR of point target analysis
Amplitude [dB]
Range

(c)

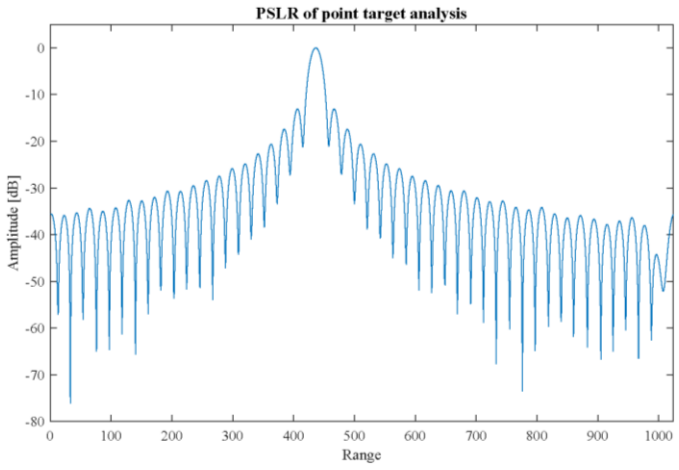
PSLR of point target analysis
Amplitude [dB]
Range

(d)

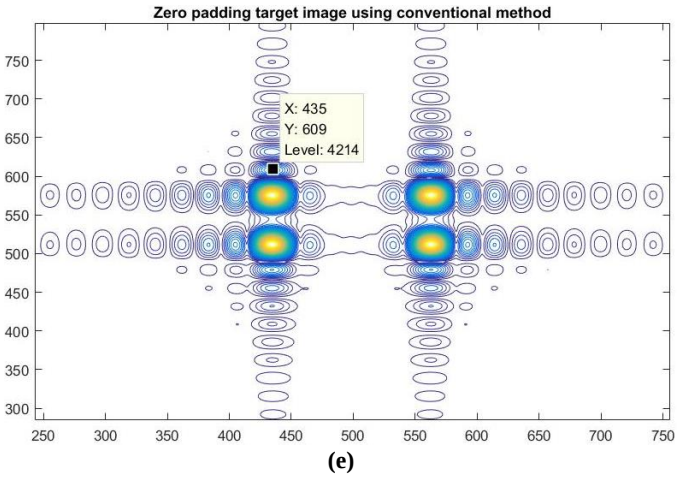
Zero padding target image using conventional method
X: 435
Y: 609
Level: 4214

(e)

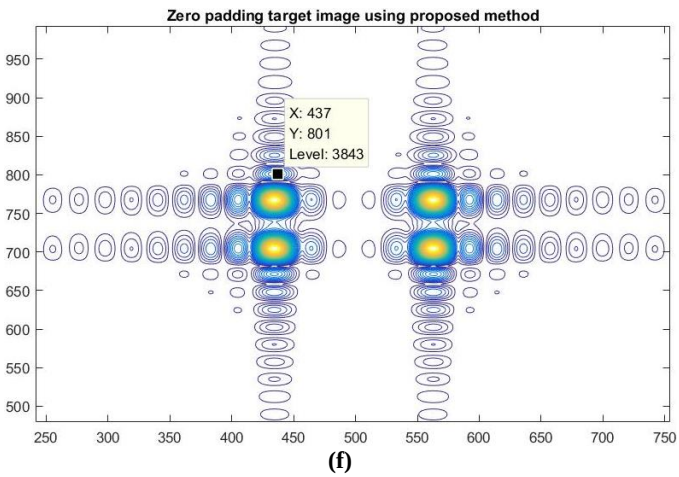
Zero padding target image using proposed method
X: 437
Y: 801
Level: 3843

(f)

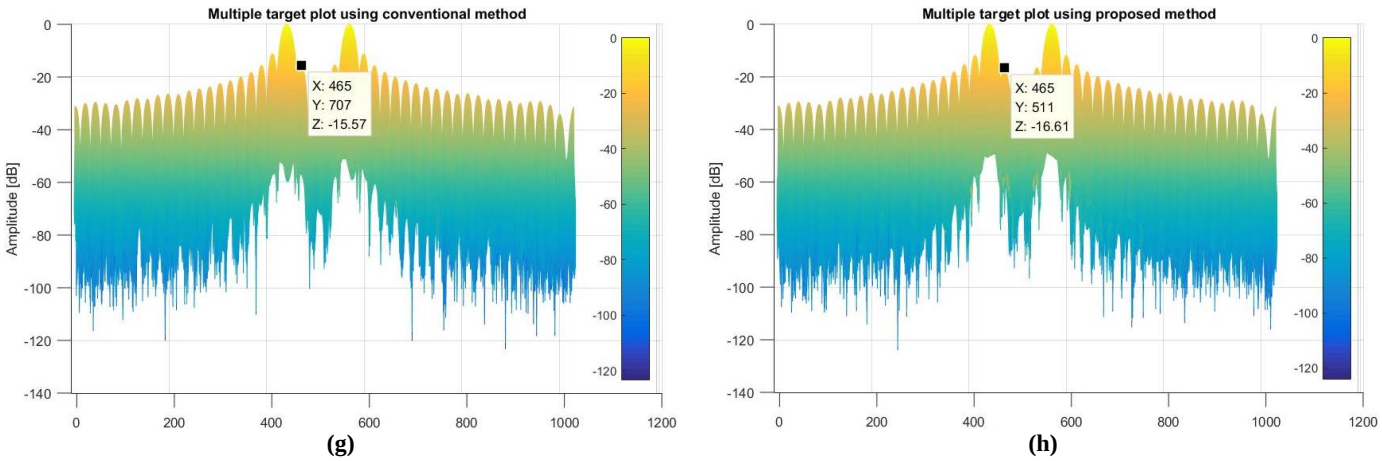

(g) (h)

Figure 5 Result of point target analysis:
(a) Conventional output; (b) Proposed DDS output; (c) IRF of conventional DDS; (d) IRF of proposed DDS;
(e) Contour plot of multiple targets from conventional DDS; (f) Contour plot of targets from proposed DDS;
(g) Multiple target IRF of conventional DDS; (h) Multiple target IRF of proposed DDS

V. CONCLUSIONS

This paper proposed a novel phase error compensation algorithm for chirp generator to improve the performance and spectrum characteristic. The proposed algorithm calculates the error coefficient of the residual noise of each DDS and compensates phase error. Numerical results show that the proposed algorithm is able to enhance the IRF characteristics and spectrum output. In case of IRF, the PSLR and ISLR of the proposed algorithm have been enhanced up to -0.2068 dB and -0.1091 dB respectively. It means the DDS is able to suppress the side lobe noise when using the proposed method. Spectrum output shows that spurious components such as spectral regrowth are reduced remarkably. Point target analysis results show that the proposed method is able to suppress side lobe and it is able to enhance the image quality. Moreover, when there are multiple targets in the area of interest, the proposed algorithm could suppress both inner and outer sidelobe level. In the case of inner sidelobe suppression has been enhanced up to -1.04 dB.

ACKNOWLEDGEMENT

Josaphat Laboratory (JMRSL) is supported in part by the European Space Agency (ESA) Earth Observation Category 1 under Grant 6613; the 4th Japan Aerospace Exploration Agency (JAXA) ALOS Research Announcement under Grant 1024; the 6th JAXA ALOS Research Announcement under Grant 3170; the Japanese Government National Budget – Ministry of Education and Technology (MEXT) FY2015-2017 under Grant 2101; Chiba University Strategic Priority Research Promotion Program FY2016-FY2018; Taiwan National Space Organization (NSPO); and Indonesian National Institute of Aeronautics and Space (LAPAN); National Institute for Environmental Studies (NIES) for ASTER images; GSI for GPS ground measurement data.

REFERENCES

[1] H. Yang, J. T. Sri Sumantyo, J.-H. An, H.-W. Jung, and J.-H. Kim, "Phase error compensation method using polynomial model for a direct digital synthesizer based chirp signal generator," *2015 IEEE International Geoscience and Remote Sensing Symposium (IGARSS)*, pp. 786-789, Jul. 2015.

[2] M. Y. Chua and V. C. Koo, "FPGA-based chirp generator for high resolution UAV SAR." *Progress in Electromagnetics Research*, Vol. 99, pp. 71-88, 2009.

[3] D. Gomez-Garcia, C. Leuschen, F. Rodriguez-Morales, J.-B. Yan, and P. Gogineni, "*Linear chirp generator based on direct digital synthesis and frequency multiplication for airborne FMCW snow probing radar*," 2014 IEEE MTT-S International Microwave Symposium (IMS 2014), pp. 1-4, 2014.

[4] L. Cordesses, "Direct digital synthesis: a tool for periodic wave generation (part 1)," *IEEE Signal Processing Magazine*, Vol. 21, no. 4, pp. 50-54, Jul. 2004.

[5] A. Samarah, "A Novel Approach for Generating Digital Chirp Signals Using FPGA Technology for Synthetic Aperture Radar Application," *Library of University of Siegen Germany*, 2012.

[6] D. Calabrese, *et al*, "New concepts and innovative solutions of the COSMO-SkyMed "Seconda Generazione" system," *2015 IEEE International Geoscience and Remote Sensing Symposium (IGARSS)*, pp. 223-226, Jul. 2015.

[7] M. Pichler, A. Stelzer, P. Gulden, C. Seisenberger, and M. Vossiek, "Phase-error measurement and compensation in PLL frequency synthesizers for FMCW sensors—I: Context and application," *IEEE Transactions on Circuits and Systems I: Regular Papers*, Vol. 54, no. 5, pp. 1006-1007, May. 2007.

[8] J. C. Curlander and R. N. McDonough, "Synthetic Aperture Radar," *Wiley Interscience*, New York, pp. 71-76, 1991.

[9] P. C. Pederson, "Digital Generation of Coherent Sweep Signal,'" *IEEE Transactions on Instrumentation and Measurement*, pp. 90-95, Feb. 1990.

[10] P. P. Sotiriadis, K. Galanopoulos, "Direct all-digital frequency synthesis techniques, spurs suppression, and deterministic jitter correction," *IEEE Transactions on Circuits and Systems*, Vol. 59, no. 5, pp. 958-968, May. 2012.